

AFIZAH AYOB¹, RAGUNATHAN SANTIAGOO¹, WAN AMIZA AMNEERA¹,
NORLI ISMAIL², AHMAD ZUHAIRI ABDULLAH³

ULTRASONIC-ASSISTED SYNTHESIS OF REACTIVE CARBOXYMETHYL CELULOSE STABILIZED NANO ZERO-VALENT IRON AND ITS APPLICATION FOR REMOVAL OF Cr⁶⁺ AND Cu²⁺ IONS

Carboxymethyl cellulose (CMC) was used in the chemical reduction using sodium borohydride to yield dispersive nano zero-valent iron (nZVI) particles as reactive and stable adsorbents. CMC-stabilized nZVI particles were characterized via UV-visible light spectroscopy, X-ray diffraction, dynamic light scattering, transmission electron microscopy, and specific surface area assisted using a probe ultrasonication dispersing tool at 50% amplitude power. High catalytic reactivity obtained in pseudo-first order reaction for Cr⁶⁺ (rate constant $K_1 = 0.0311 \text{ min}^{-1}$) and pseudo-second order for Cu²⁺ (rate constant $K_2 = 0.0946 \text{ g} \cdot \text{mg}^{-1} \cdot \text{min}^{-1}$) indicated that colloidal stability of nZVI particles can be achieved with a stabilizer for the removal of toxic contaminants.

1. INTRODUCTION

Human life style has been improving extensively in the last few decades with the progresses in science and technology. However, industrialization has increased the generation of waste in various ways with the concomitance of adorning human life. Environmental pollution is one of the major consequences of technological advancement. Water and soil pollution are the two serious issues posing great threat to the environment and, thus, to human life.

Heavy metals are mainly responsible for this pollution. In small amount, some of these heavy metals promote a healthy diet but excess levels can be lethal. Among many

¹School of Environmental Engineering, Universiti Malaysia Perlis, Jejawi, 02600 Arau, Perlis, Malaysia, corresponding author A. Ayob, e-mail: afizah@unimap.edu.my

²School of Industrial Technology, Universiti Sains Malaysia, 11800 Minden, P. Pinang, Malaysia.

³School of Chemical Engineering, Universiti Sains Malaysia, 14300 Nibong Tebal, P. Pinang, Malaysia.

toxic metals in the environment, chromium and copper occur regularly at contaminant zone, being categorized as primary contaminants. Those heavy metals can be introduced to the water and soil body from sources such as mining and smelting industries, dyes and pigments, sewage sludge, petrochemical industries, coating and painting manufacturing, fuel production, fertilizer and pesticide applications, and sometimes uncontrolled or intentional releases to the environment [1–3]. These toxic metals can be ingested into the human body by water, and from soil or air if inhaled. The carcinogenic nature of Cr^{6+} compounds was first recognized in the late 19th century when detected in Scottish chrome pigment workers. Cr^{6+} is toxic and carcinogenic when inhaled by up to 1000 fold [3]. At short-term exposure above the maximum pollutant level, Cr causes ordinary irritation to the skin and stomach. Long-term exposure leads to dermatitis, liver failure, kidney circulation, and death in large doses. Excessive intake of Cu by humans may lead to severe mucosal irritation and corrosion, widespread capillary damage, hepatic and renal failure, and irritation of the central nervous system, followed by depression. Cu in water has been found to damage marine life which effects on fish and other creatures including destruction of gills, liver, and kidneys [4].

Nano zero-valent iron (nZVI) technology is regarded the first generation of nanoscale remediation emerging technologies [5, 6]. Studies implement and diversify advanced nanotechnology to remove chemical and biological substances in the contaminated environment. However, due to significant variations in pollutant chemistry, numerous removal pathways using nZVI particles were determined. Sorption, co-precipitation, surface and mediated chemical reduction and complexation are included [7]. These processes are based on the standard reduction potentials (E^θ) or the availability of electrons within the system. Oxidation states and reduction potentials of nZVI determine the role and function of nZVI particles as excellent reducing agents.

nZVI which is referred to as metallic iron (Fe^0), is highly capable to corrosion in aqueous system [3, 8]. This corrosion mainly occurs via an electrochemical processes, at both anodic and cathodic reactions. The anodic reaction includes the dissolution of nZVI leading to soluble ionic complexes or insoluble oxide/hydroxide. In addition, high reactive surface area of nZVI particles significantly accelerates reduction through the generation of H_2 :



This reaction incites local conditions much better than equilibrium and beneficial to contaminant removal. Yet, as the kinetics of nZVI oxidation is extremely rapid, corrosion will develop even under restrained conditions. However, the intrinsic reactivity of

pure nZVI significantly decreases during the reaction. This phenomenon is due to agglomeration of nZVI particles and adhesion caused by the van der Waals and magnetic forces, which affect the reactive surface area and lead to decrease the rate of contaminant removal [9]. In addition, surface passivation greatly hinders electron transfer to target contaminants. Therefore, surface stabilization with polymer/surfactant on the nZVI particles surface could overcome these difficulties. The stabilizers attached to the nZVI prevent the particles from aggregation through steric and/or electrostatic stabilization mechanisms, leading to improved physical stability, better mobility in targeted zone and greater specific surface area.

In the present study, ultrasonic-assisted preparation of carboxymethyl cellulose (CMC)-stabilized nZVI particles has been reported through chemical reduction to remove Cr^{6+} and Cu^{2+} ions from aqueous solution. The morphology and particle-stabilizing mechanisms of CMC-stabilized nZVI have been examined.

2. EXPERIMENTAL

All chemicals were of analytical or laboratory reagent grades and were used as received. Ferrous sulfate heptahydrate (>99.9% $\text{FeSO}_4 \cdot 7\text{H}_2\text{O}$) was purchased from the Fisher Scientific, CMC ($MW = 90 \text{ K}$) from Acros Organic, sodium borohydride (>98.0% NaBH_4), sodium chromate tetrahydrate (>99.9% $\text{Na}_2\text{CrO}_4 \cdot 4\text{H}_2\text{O}$) and copper sulfate pentahydrate (>99.99% $\text{CuSO}_4 \cdot 5\text{H}_2\text{O}$) from Sigma Aldrich.

Synthesis of CMC-stabilized nZVI particles. The CMC-stabilized nZVI particles were synthesized by a modified chemical reduction method [10]. 1.0 dm^3 of CMC stock solution at the concentration of 1.2 wt. % was prepared by dissolving the CMC powder in deionized water. The Fe concentration was kept constant at 2.0 g/dm^3 , and the CMC: Fe^{2+} molar ratio was fixed at 0.0034. NaBH_4 was adjusted in double excess of the stoichiometric requirement ($\text{BH}_4^-:\text{Fe}^{2+}$ molar ratio of 2:1) and was titrated at a fast rate of $5 \text{ cm}^3/\text{min}$ for a complete reaction with iron at temperatures between $10 \text{ }^\circ\text{C}$ and $18 \text{ }^\circ\text{C}$ because of the competing reaction between BH_4^- and water. A clear yellow color changed to black during the instantaneous reduction immediately after the first drop of BH_4^- . The emergence of particles was accompanied by the generation of hydrogen bubbles. To avoid agglomeration, the more powerful tool in dispersing the CMC-stabilized nZVI particle was chosen in the study. Probe ultrasonication was conducted to the CMC-stabilized nZVI suspension for around 15 min by using a probe horn sonicator at 50% amplitude power (Branson Digital Sonifier, 450). The suspension was then immediately used for the characterizations.

Characterization of CMC-stabilized nZVI particles. A Shimadzu UV-Vis spectrophotometer (UV-1601 PC) was used to record the adsorption spectra of the CMC-

-stabilized nZVI particles upon reduction with NaBH_4 . The suspension of 2.0 g/dm^3 of CMC-stabilized nZVI particles, the bare suspension and 1.2 wt. % solution of CMC alone were examined at 200 to 700 nm. XRD patterns were determined using a Bruker AXS powder diffractometer with the Bragg–Brentano geometry equipped with a curved graphite monochromator in the diffracted beam arm and Cu-K_α radiation ($k = 0.15406$). The samples were examined within the range of 2θ values from 5° to 90° using a step size of 0.034° , a counting time of 107.4 s per step at 25°C .

The structure of the CMC-stabilized nZVI particles was characterized using a Zeiss LIBRA 120 TEM microscope. Bulk drops of the suspension were placed on the carbon-coated copper grid, and filter paper was used to remove the excess sample. The residual sample attached onto the grid was then dried overnight under a N_2 flow before viewed using transmission electron microscopy (TEM). Dynamic light scattering (DLS) is a technique to reliably measure the width and the Z-averaged translation diffusion coefficient (D_z), which is sensitive to the intensity of scattered light. The particle size distribution of DLS is derived from a deconvolution of the measured intensity autocorrelation function of the sample. Herein, the measurement was performed at 633 nm (25°C) using a Malvern Zetasizer NanoZS instrument (Worcestershire, UK). The dispersant refractive index (RI) was set to 1.33 and 2.90 for the dispersant (water) and the nZVI particle ($\text{Fe}^0/\text{Fe}_3\text{O}_4$) core-shell structure, respectively. The black, freshly prepared, CMC-stabilized nZVI suspension was diluted into clear solutions at dilution factor of up to 100–150, before the measurement at 90° angle and was positioned at 1.25 mm. The diluted samples were used to avoid the multiple scattering that could interfere with the data interpretation.

The specific surface area (SSA) was determined using a volumetric gas adsorption instrument (Micromeritics ASAP 2000 Series, Germany) at 77. SSA (m^2/g) can be calculated from the following equation:

$$\text{SSA} = \frac{\text{surface area}}{\text{mass}} = \frac{\pi d^2}{\frac{\pi}{6} d \rho} \quad (3)$$

where ρ is the density of the iron particles (7.8 g/cm^3) and d is the primary particle diameter (m). Solid pure nZVI particles were assumed to have no internal surface and to have spherical geometry.

Kinetic removal of Cr^{6+} and Cu^{2+} in aqueous solution. A stock solution of 500 mg/dm^3 Cr^{6+} and Cu^{2+} was prepared by dissolving $\text{Na}_2\text{CrO}_4 \cdot 4\text{H}_2\text{O}$ and $\text{CuSO}_4 \cdot 5\text{H}_2\text{O}$, respectively, in ultrapure water. Fresh CMC-stabilized nZVI suspensions of the concentration

of 2.0 g/dm³ was examined at CMC:Fe²⁺ molar ratio of 0.0034 and the CMC concentration was kept constant at 1.2 wt. %. The kinetic test was initiated by injecting 10 mg/dm³ of stock solution (Cr⁶⁺/Cu²⁺) into 12 cm³ samples of the nZVI particle suspension, which were placed in 13 cm³ glass vials. The solution was adjusted to pH of 4.5–5.5. The injected suspension was then agitated at 30 °C on a rotator of 130 rpm, zero head space, the collection time of 0, 15, 30, 60, 120, 180, and 240 min. The kinetic tests were conducted at least in triplicate to ensure measurement repeatability. The control experiments were conducted at similar experimental conditions. The samples were transferred to centrifuge tubes, centrifuged at 3500 rpm for 10 min, and immediately filtered using a 0.45 μm Whatman membrane filter paper before further analyses. The concentrations of Cr⁶⁺ ions were determined by the colorimetric method (DR 890) with 1,5-diphenylcarbohydrazide at 540 nm. Concentrations of Cu²⁺ ions were determined using an atomic absorption spectrophotometer (Analyst 100 PerkinElmer). To avoid the interference caused by aging effects, the CMC-stabilized nZVI was always freshly made before being used.

The percentage of pollutants removed (R_p) by the adsorbent was calculated using the following equation:

$$R_p = \frac{C_0 - C_e}{C_0} \times 100\% \quad (4)$$

To calculate the removal capacity for CMC-stabilized nZVI particles, the mass balance calculation was used:

$$q = \frac{(C_0 - C_e)V}{W} \quad (5)$$

where C_0 and C_e are the initial and equilibrium concentrations of pollutant ions (mg/dm³) in the solution, respectively, q is the reduction capacity (mg/g), V is the volume of the solution (dm³), and W is the mass of the nZVI particles (g).

The kinetic data were analyzed using pseudo-first order (PSO) and pseudo-second order (PSO) equations.

For the pseudo-first order equation we have:

$$\log(q_e - q) = \log q_e - \frac{K_1 t}{2.303} \quad (6)$$

where K_1 (min⁻¹) is the rate constant of the PFO model, q is the amount of solute adsorbed on the adsorbent at time t (mg/g), and q_e is the amount of solute adsorbed on the

adsorbent at the equilibrium state per unit weight of adsorbent (mg/g) for the boundary conditions from $t = 0$ to $t > 0$ (and from $q = 0$ to $q > 0$).

The rearranged PSO equation that follows the linear time dependence is as follows:

$$\frac{t}{q} = \frac{1}{K_2 q_e^2} + \frac{1}{q_e} t \quad (7)$$

where we assume that

$$h = K_2 q_e^2 \quad (8)$$

where K_2 ($\text{g} \cdot \text{mg}^{-1} \cdot \text{min}^{-1}$) is the rate constant of the PSO reaction and h is the initial sorption rate ($\text{mg} \cdot \text{g}^{-1} \cdot \text{min}^{-1}$). The rate constants K_1 and K_2 were calculated from the slopes of the plots based on Eqs. (6) and (7), respectively. The h value can be determined from the intercept of the plot t/q versus t (Eqs. (7) and (8)).

In a similar experiment at initial $\text{Cr}^{6+}/\text{Cu}^{2+}$ concentrations of 7, 10, 15, 20, and 30 mg/dm^3 , the adsorption isotherm data were fitted to the Langmuir equation and the Freundlich model.

The Langmuir equation is as follows:

$$\frac{C_e}{A_m} = \frac{1}{K_L} \times \frac{1}{b} + \frac{1}{b} C_e \quad (9)$$

where C_e is the equilibrium concentration (mg/dm^3), A_m is corresponding aqueous phase concentration (mg/g), K_L is the Langmuir maximum capacity (mg/g), and b is the Langmuir binding coefficient (dm^3/mg). Therefore, the values of b and K_L were obtained by a linear straight fitting (Eq. 9) according to respective equilibrium adsorption data. A further analysis of the equation can be expressed in terms of the separation factor, a dimensionless equilibrium constant:

$$R_L = \frac{1}{1 + bC_0} \quad (10)$$

For the Langmuir isotherm, a thermodynamic parameter, the standard free energy, ΔG° , corresponding to transferring of 1 mole of solute from solution onto the solid–liquid interface, can be calculated from:

$$\Delta G^\circ = -RT \ln K_L \quad (11)$$

where R is the universal gas constant equal to $8,314 \text{ J} \cdot \text{mol}^{-1} \cdot \text{K}^{-1}$ and T is temperature (K).

The Freundlich model can be applied to non-ideal sorption of heterogeneous surfaces and multilayer sorption:

$$A_m = K_F C_e^n \quad (12)$$

or in a logarithmic form

$$\ln A_m = \ln K_F + \frac{1}{n} \ln C_e \quad (13)$$

where K_F is the Freundlich isotherm constant, being the measure of the adsorption capacity, the other symbols have its usual meaning.

A plot of $\ln A_m$ versus $\ln C_e$ should be a straight line with a slope $1/n$, and the intercept $\ln K_F$. The value of n depends on the intensity of adsorption. $n > 1$ represents favorable adsorption conditions.

3. RESULTS AND DISCUSSION

3.1. CHARACTERIZATIONS OF CMC-STABILIZED nZVI PARTICLES

3.1.1. UV-VIS SPECTROSCOPY

The UV-Vis absorption spectra of metal colloids were recorded before and after reduction with $NaBH_4$ (Fig. 1). The stabilizer, CMC 90K alone, showed no absorbance peak in the range 200–700 nm (spectrum not shown). CMC- Fe^{2+} suspension demonstrated a small hump at 290, 300, and 477 nm in the spectrum of the colloid before reduction, and solution appeared transparent. The possible of these humps may be the adsorption and electronic coupling of ferrous ions with deionized water [11].

During the reduction of CMC-stabilized nZVI suspension with BH_4^- pH increased to ca. 8.6 and the color of the solution changed immediately to black, giving rise to changes in the absorbance profile. The peaks were observed at 298 and 511 nm in spectrum (b) which provides an instant indication of the decrease in particle sizes and formation of metal (Fe^0) colloids due to the stabilization process [11]. Nevertheless, the actual particle size distribution of CMC-stabilized nZVI particles was not clarified in this method. However, based on literature, in such cases, the absorption edge significantly shifted with decreasing $\alpha-Fe_2O_3$ nanoparticle sizes at a maximum peak of 460 nm, which was predicted within the 1 to 60 nm range [12]. Therefore, the peak observed at 511 nm may be due to the nanoscale size, poorly crystalline-amorphous particles obtained after the reduction process, extended with ultrasonication (Fig. 1).

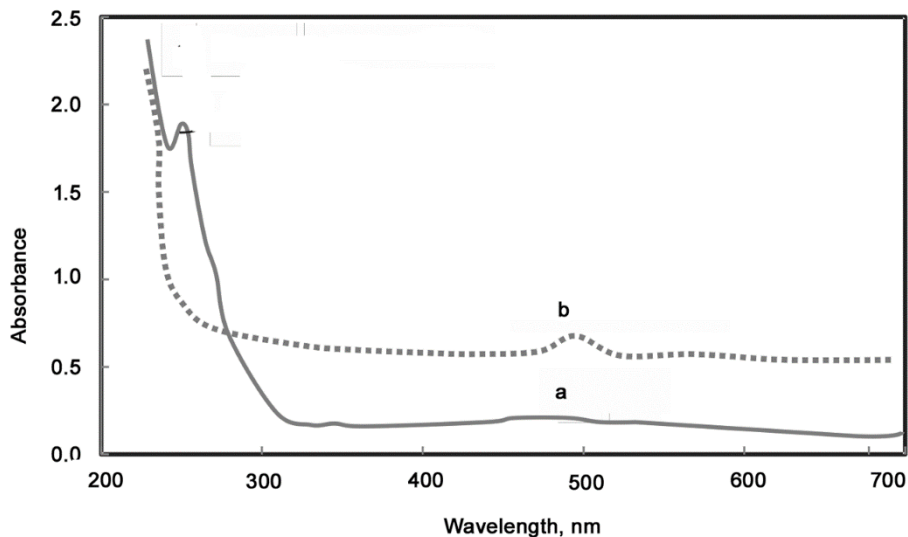


Fig. 1. UV-Vis spectra for: a) CMC-Fe²⁺ suspension before reduction, b) CMC-stabilized nZVI particles after reduction with NaBH₄

The CMC acid dissociation constant (pK_a) = 4.3 was due to the contribution of the negatively charged polymeric moieties. The $-OH$ is dominant when pH of the colloid suspension is lower than pK_a [13]. Therefore, in this study, the CMC carboxylic groups were presumably fully disassociated to bind strongly with Fe²⁺ at pH of 8.6. This occurrence was followed by electrostatic and Lewis acid-base interactions to stabilize the nZVI suspension. The absorbance intensity decreased dramatically at higher wavelengths which corresponded to the reduction process (Fig. 1). The almost monotonically, somewhat exponentially decayed band was observed in spectrum (b) as the wavelength increased. This band type with deteriorated electronic structure was probably due to the nZVI particles that existed not as single atoms but rather as clusters. Simultaneously, with the ionization of the carboxylate groups on the elemental surface, the nZVI particles dispersed and formed distinctly small semi-crystalline-amorphous grains. Furthermore, particle-particle interactions can be avoided to exploit the full potential of the CMC stabilized-nZVI particles in the aqueous suspension.

3.1.2. X-RAY DIFFRACTION (XRD)

The XRD patterns for non-stabilized and CMC-stabilized nZVI particles are shown in Fig. 2. Both patterns obtained for freshly synthesized nZVI suspension confirm that the particles were formed without impurities. No obvious peak originating from crystalline iron was observed in both samples, suggesting that the nZVI species were dispersed, forming very small crystallites with size below the detection limit of X-ray diffraction. Only one major spinel structure peak at 2θ of 44.65° (1,1,0) was attributed to the zero-valent iron (α -Fe) in pure non-stabilized nZVI particles (spectrum (a)). Other

important peaks at 64.99° (2,0,0), and 82.33° (2,1,1) characteristic of $\alpha\text{-Fe}$ were invisible which might be due to the nature of amorphous phase of nZVI. The Bragg peaks observed at 2θ of $20\text{--}35^\circ$ indicate the presence of iron hydroxides at the crystalline phases.

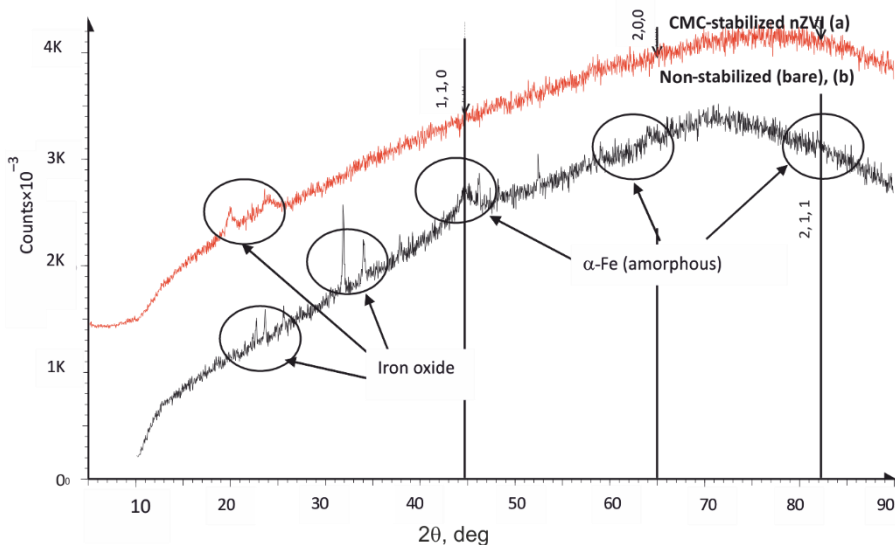


Fig. 2. XRD patterns of: a) non-stabilized, b) CMC-stabilized particles

Significant changes were observed when nZVI particles were stabilized with CMC. The broadening of the diffraction line for CMC-stabilized nZVI particles provided evidence of the poorly semi-crystalline amorphous phase (spectrum (b)). The observed phase could also be produced during ultrasonication of the sample that breaks down the CMC-stabilized nZVI particles to become poorly semi-crystalline.

Furthermore, phenomena observed in the diffraction spectrum (b) were ambiguous. The expected characteristic peak of metallic nZVI iron ($\alpha\text{-Fe}$) disappeared. This behavior was attributed to the random loading of nZVI particles (2.0 g/dm^3) which were too small to be visible under XRD analysis. The presence of any crystalline species at less than 5 wt. % of Fe was almost impossible to be detected [14]. In addition, the intensity of the diffraction spectrum was quantitatively proportional to the amount of nZVI particles. Broad peak attributed to iron hydroxides at 2θ of $20\text{--}35^\circ$ (hematite, $\gamma\text{-Fe}_2\text{O}_3$ or magnetite, Fe_3O_4) were observed for CMC-stabilized nZVI particles (spectrum (b)). Therefore, CMC 90K may protect the surrounding nZVI particles from further corrosion and can inhibit them from being oxidized under ambient air. The absence of reflections originating from iron hydroxides in the XRD patterns, however, did not indicate its total absence in the CMC-stabilized nZVI sample. The XRD spectrum of a given material reflects the crystallinity/amorphously phase signal, rather than its oxidation state. Iron

oxides coating the nZVI surface were found to create an amorphous layer. Its thickness was probably too low and well below the detection range of XRD detection. In this case, the line profiles were not capable of providing information on the true size and shape of both types of nZVI particles.

3.1.3. TRANSMISSION ELECTRON SPECTROSCOPY (TEM)

TEM analysis was performed to investigate the size, shape, and morphology of non-stabilized and CMC-stabilized nZVI particles (Fig. 3).

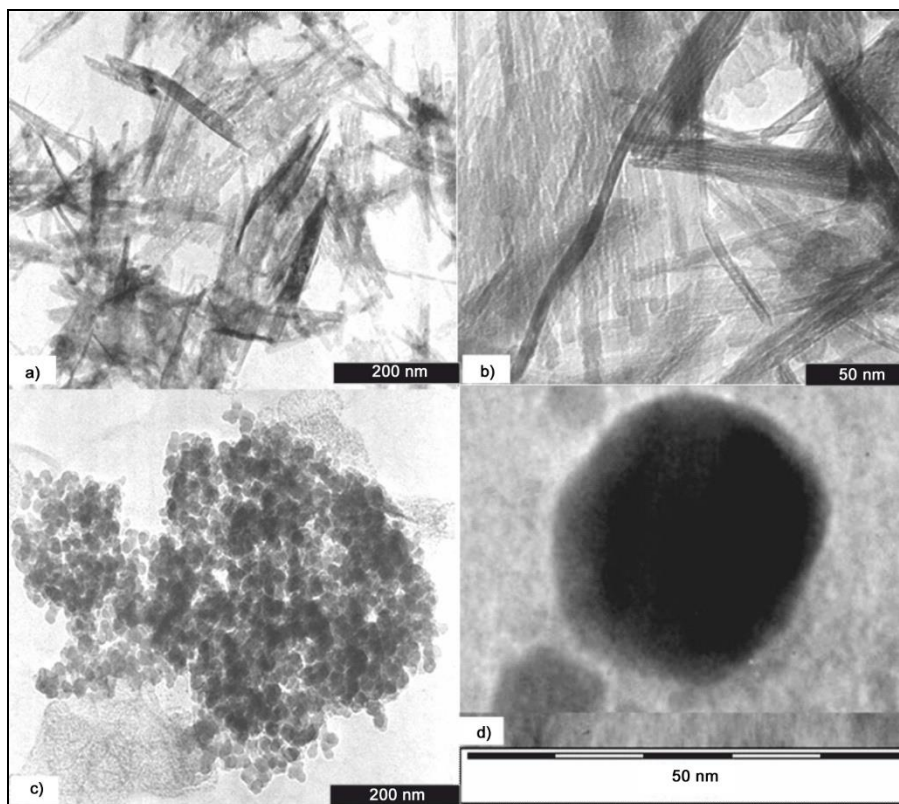


Fig. 3. TEM images of: a), b) non-stabilized, and c), d) CMC-stabilized nZVI particles at various magnifications

For non-stabilized nZVI, isolated individual particles were difficult to locate (Fig. 3a). The highly transparent particles enabled TEM to discern a finer substructure. Instead, the non-stabilized nZVI particles appeared to be fused to each other, thereby forming a needle-like morphology that was clearly agglomerated (Fig. 3b). This needle-like structure could originate from strong magnetic dipole-dipole attractions between the non-stabilized individual nZVI particles, when the ultrasonication was not used. The

local non-stabilized magnetic nZVI particles were also likely to occur after drying or during TEM visualization. Due to the same reason, a native oxide shell on the surface of those particles could not be noticed (Figs. 3a, b).

The CMC-stabilized nZVI particles were rather polydispersed, and no aggregation was observed in the solution (Fig. 3c). CMC-stabilized nZVI particles were mainly spherical and almost all individual particles were less than 100 nm. This observation could be due to the rapid nucleation and crystal growth upon slightly higher amount of BH_4^- in the reduction process. It then reduced CMC-complexed Fe^{2+} ions to elemental Fe. The sizes of the rectangular and/or irregularly shaped particles were generally larger than those of the round particles. In contrast to He and Zhao [9] they observed much larger aggregates at the lower CMC: Fe^{2+} molar ratio of 0.0062 at 0.1 g/dm³ of Fe. This indicates that the optimum CMC: Fe^{2+} molar ratio is required to achieve particle stabilization.

A clear contrast between the core and thin oxide shell was observed for CMC-stabilized nZVI particles (Fig. 3d). The core was composed of crystalline grains (Fe^0), whereas the shell, apparently brighter, was amorphous. The outer shells had significantly variable thickness from 6 nm to 3 nm. This variation was caused by forces that hindered formation of the crystalline core. Thus, the small radii of the nZVI particles and the curvature of the oxide shell contributed to the irregular thickness of the oxide shell. On the contrary, the arrangement of the metallic core-oxide phase depends on the method of synthesis, particle size distribution, and storage conditions. In addition, the reaction of the residual boron caused by an excess amount of BH_4^- in the oxide layer partly caused defects in the formation of the oxide layer. This unique configuration protected the core iron against further oxidation and provided means for mass and charge transport. Therefore, the core possessed the reductive and sorptive characteristics of metallic iron and the coordinative properties of iron oxides.

The surface oxide layer of nZVI particles (Fig. 3d) was oxidized in aqueous solution and was probably in the form of FeOOH , in which its reactive site would actively be involved in removal processes. Alternatively, in a similar manner, the layer acted as an iron (oxyhydro) oxide for surface adsorption to bind with contaminants in water media. Potentially, the defective effect caused the specific reactivity of CMC-stabilized particles based on their functions in the environmental remediation processes [15].

3.1.4. DYNAMIC LIGHT SCATTERING (DLS)

DLS analysis offers some advantages over TEM by measuring the hydrodynamic size of particles from the original suspension at a much larger volume of ca. 0.5 cm³ per sample. The TEM measurements (based on the scattering and diffraction of electrons) determined only the inorganic electron-dense Fe core, and the layer of the surrounding CMC could not be seen due to the poor contrast [16]. The size distribution obtained from DLS measurements corresponds to a higher average than the one obtained from XRD or TEM measurements due to the intrinsic sensitivity of the technique to

small aggregates present in the dispersion [16]. DLS technique is used for finer particles ranging from 3 to 6 μm . The CMC-stabilized nZVI suspensions used usually require a homogenization protocol such as probe ultrasonication (at around 20 min), to break up larger aggregates prior to DLS analysis. On the contrary, longer ultrasonication period can breakup physically welded agglomerates of CMC-stabilized nZVI particles, thereby skewing the true particle size distribution of the sample.

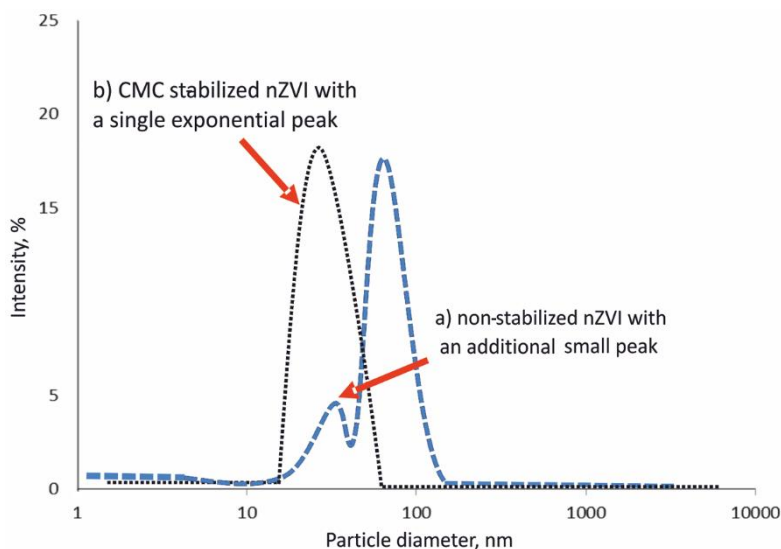


Fig. 4. Particle size distribution of: a) non-stabilized nZVI, b) CMC-stabilized nZVI particles based on DLS analysis

The log-normal particle size distributions were based on the peak intensity for the non-stabilized and CMC-stabilized particles (curve a, Fig. 4). The obtained poly-dispersibility (PDI) for the non-stabilized suspension was 0.361. Their recorded mean diameter (Z-average) was 185.1 nm accompanied by the formation of an additional small peak. Although, the PDI was relatively favorable, the small peak segment represented the non-homogeneous suspension with agglomerated particles. The distribution corresponded to the aggregation of non-stabilized nZVI population to large micron-sized aggregates. The fundamental forces that dominated the aggregation included the van der Waals attraction, Brownian motion, electrical repulsion, electrosteric repulsion, and magnetic attraction [9]. It means, no energy barrier was present to resist aggregation. Without ultrasonication, the aggregation of unmodified portions, when prolonged, can increase the individual sizes of the particles (curve a, Fig. 4). Therefore, the non-stabilized nZVI particles would be rendered immobile by the source contaminants, making them unsatisfactory for remediation strategies.

The PDI obtained for CMC-stabilized nZVI particles was 0.151, with a single exponential and narrow peak, after ultrasonication with power of 50% (curve b, Fig. 4). This suggests that CMC-stabilized nZVI particles were evenly discrete and relatively stable over time. The CMC-stabilized nZVI suspension particles yielded a Z-average diameter of ca. 45 nm. The CMC-stabilized nZVI suspension particles yielded a Z-average diameter of ca. 45 nm (curve b, Fig. 4). The thickness of CMC layer was also counted as a true size of CMC-stabilized nZVI suspension particles. Majority of the particles were still in the nano-range (smaller than 100 nm). Probe ultrasonication tool was sufficient to generate a high frequency ultrasound which randomly destroyed the aggregates of the CMC-stabilized ZVI particles. It resulted in the decrease of their size which did not affect the stability of the dispersion, rather increasing it, due to differential sedimentation because of the polydispersity of CMC-stabilized nZVI particles [6].

However, the result is inconsistent with Greenlee and Hooker [17] as they obtained the smallest modal particle diameter of 5.3 ± 2.5 nm, at a smaller CMC: Fe^{2+} molar ratio of 0.0005 using DLS analysis. Their small particle diameter could be due the excess of iron salt (including CMC) which had been washed and removed, prior to the analysis. In addition, the degree of polymerization and carboxylic groups of CMC can be attributed to the specific natural affinity for iron oxide, which was required for the stabilization of nZVI particles. Accordingly, Rayleigh's approximation indicates that the intensity-average and diffusivity based on the DLS were sensitive to aggregation, although a small portion of the particle in the population were aggregated, which justified the obtained Z-average diameter [18].

3.1.5. SPECIFIC SURFACE AREA (SSA)

The SSA of nZVI particles is one of the main factors affecting the physical and chemical properties of nanoparticles. The BET surface area measurement yielded fairly higher SSA values ranging from 3.2 to 18.4 m^2/g for both non-stabilized and CMC-stabilized nZVI particles. Evidently, the presence of CMC suppressed the growth and aggregation of nZVI particles, and, thus maintained a higher SSA. In comparison, some of the SSA values for the nZVI particles produced by the same borohydride reduction method reported from previous literature were 36.5 m^2/g [19], and 19.0 m^2/g [20].

The actual SSA value was determined at 18.4 m^2/g (Eq. 3), which gives a meaningful value of CMC-stabilized nZVI particle size of around 41.7 nm. The SSA value from the BET analysis was inversely related to the nZVI particle radius as suggested Eq. (3). This theoretical diameter from SSA is in agreement to the Z-average diameter recorded in the DLS measurement. The significant difference of SSA value for both non-stabilized and CMC-stabilized nZVI obtained in this study, yet no such discussions in regards to CMC: Fe^{2+} molar ratio or effect of probe ultrasonication is drawn here. During the synthesis, the molar ratio of CMC: Fe^{2+} is of a particular significance as it regulates iron nucleation and particle growth but it is not necessarily by proportional increase in SSA.

In addition, as previously discussed, the structure of the surface layer of the CMC-stabilized nZVI particles can be attributed to the oxidation and hydration phenomena. Exposure to air unintentionally happened during the synthesis or storage. Thus, rapid oxidation on the CMC-stabilized nZVI particle surface may occur during the washing process, thereby significantly decreasing the SSA value. Herein, a higher SSA value indicates an increase in the total amount of iron on the nZVI surfaces. The active site for removal was the iron surface itself; thus, samples with high surface area higher exhibited greater reaction rates with contaminants.

Pore sizes were determined using the Barret–Joyner–Halenda (BJH) method. The adsorption data revealed no evidence of microporosity (less than 2 nm). The average pore diameters were 7.1 and 10.0 nm for non-stabilized and CMC-stabilized nZVI dry powder particles, respectively. The average pore diameter in both nZVI particle samples corresponded mainly to mesopores ($2 \text{ nm} < d < 50 \text{ nm}$). These pore diameters were intuitively correlated with both adsorption and kinetic behavior. The mesopore structure increased the surface area, number of hydroxyl groups, and organic matter available for adsorption of heavy metal ions [21].

In the study, organic matter refers to the stabilizer introduced during the synthesis. Higher pores diameters of 10.0 nm relative to the size of the stabilizer particles were preferred, which can contribute to an even distribution of CMC surface moieties and pore blockage control. Small mesopores limit the kinds of ions and molecules that could permeate the interior of the nZVI particles. Therefore, the result of this characterization could greatly expand the potential of CMC-stabilized nZVI particles as adsorbents.

3.1.6. STUDY OF BATCH REMOVAL OF Cr^{6+} AND Cu^{2+} IONS

Removal efficiencies of 10 mg/dm^3 of Cr^{6+} or Cu^{2+} ions by CMC-stabilized nZVI particles were determined as 87.65% and 94.65%, respectively, over a period of 4 h under equilibrium conditions (Fig. 5). Whereas, for non-stabilized nZVI particles they amounted 37.50% for Cr^{6+} and 46.79% for Cu^{2+} ions with further increase in contact time. The Cr^{6+} and Cu^{2+} removal efficiencies were initially high, probably due to the larger surface area of the CMC-stabilized nZVI particles. This enhancement corresponds to a higher adsorbent concentration proportional to the increase in the number of binding sites, thereby resulting in improved $\text{Cr}^{6+}/\text{Cu}^{2+}$ removal.

The kinetic experimental data were fitted to both PFO and PSO models (Fig. 6) [4]. Based on the correlation coefficients R^2 , the PFO model provides a better prediction for the adsorption of Cr^{6+} ions in the presence of CMC-stabilized nZVI particles (Table 1). The recorded Cr^{6+} removal kinetic rates K_1 were 0.0311 min^{-1} and $6.2181 \times 10^{-3} \text{ min}^{-1}$, for the CMC-stabilized nZVI and non-stabilized nZVI particles, respectively. Therefore, at the same concentration (2.0 g/dm^3) of the CMC-stabilized nZVI particles, removal efficiency of Cr^{6+} ions was approximately five times higher than that of non-stabilized nZVI particles.

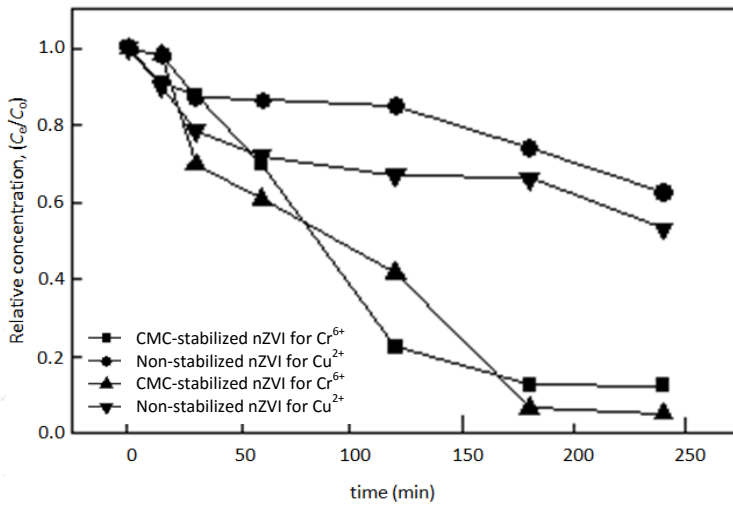


Fig. 5. Removal of Cr^{6+} (pH 5.5) and Cu^{2+} (pH 4.5) by CMC-stabilized nZVI and non-stabilized nZVI particles measured as relative concentration of C_t/C_0

Table 1

PFO and PSO values for the removal of Cr^{6+} and Cu^{2+} at CMC: Fe^{2+} molar ratio = 0.0034 of 2.0 g/dm^3 of CMC-stabilized nZVI particles

nZVI	PFO				PSO				
	K_1 [min^{-1}]	q_e		R^2	K_2 [$\text{g} \cdot \text{mg}^{-1} \cdot \text{g} \cdot \text{min}^{-1}$]	h [$\text{mg} \cdot \text{g}^{-1} \cdot \text{g} \cdot \text{min}^{-1}$]	q_e		R^2
		Exp.	Theoret.				Exp.	Theoret.	
Cr^{6+} removal									
CMC-stabilized	0.0311	2.5309	4.3830	0.8677	5.1349×10^{-4}	0.0397×10^{-3}	–	–	0.2058
Non-stabilized	6.2181×10^{-3}	–	–	0.9364	1.6256×10^{-3}	0.0137	–	–	0.1010
Cu^{2+} removal									
CMC-stabilized	0.0281	–	–	0.7734	0.0946	2.3595	4.9994	4.9730	0.9995
Non-stabilized	6.6787×10^{-3}	–	–	0.7920	0.0116	0.0642	–	–	0.9030

In Cu^{2+} removal, the PFO kinetic model showed poorly adjusted R^2 values (0.7734, 0.7920), whereas that of PSO yielded higher correlation coefficients ranging from 0.9030 to 0.9995 (Table 1). Considering the particle size difference between non-stabilized and CMC-stabilized nZVI solution, the reactivity difference between these two particles could be even greater. Compared to the non-stabilized nZVI suspension, the fresh CMC-stabilized nZVI offered eight times greater K_2 value of the removal of Cu^{2+} . The K_2 value for CMC-stabilized nanoparticles was $0.0946 \text{ g} \cdot \text{mg}^{-1} \cdot \text{min}^{-1}$ based on DLS

diameter of 45 nm. In this case, the nano scale particles after ultrasonication can regulate the redox reactions in the solution and increase the removal rate constant K_2 .

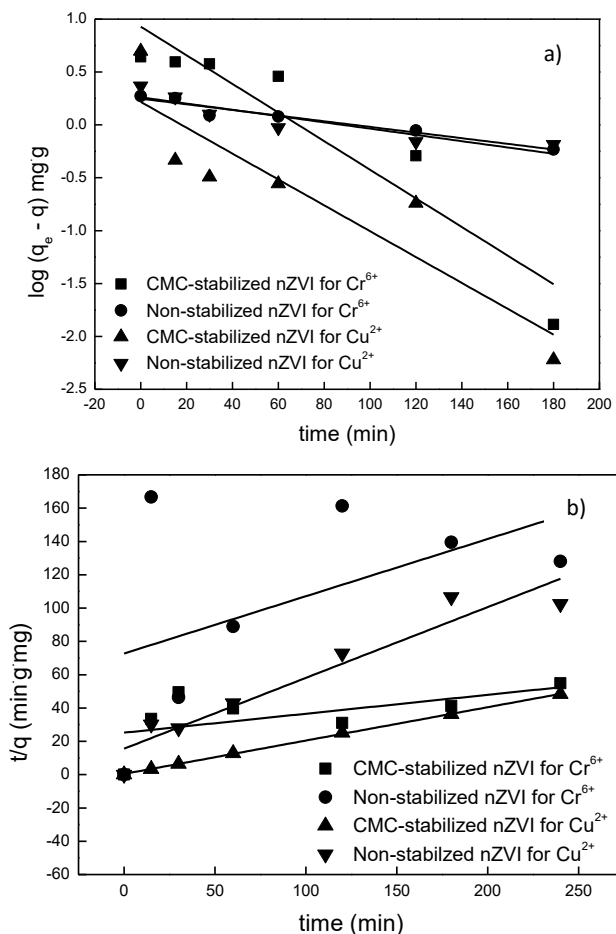
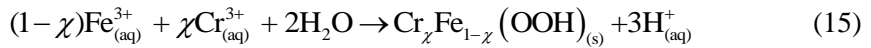


Fig. 6. Kinetic models of: a) PFO, b) PSO for the removal of Cr^{6+} and Cu^{2+} at the concentration of 2.0 g/dm^3 of CMC-stabilized nZVI particle suspension

Predicting the rate constant of adsorption for nZVI system is probably the most important factor in adsorption system design, with adsorbate residence time and the reaction order controlled by the system's kinetics. For the Cr^{6+} removal according to PFO reaction, the calculated q_e values were much higher than those obtained experimentally (Table 1). However, the equilibrium adsorption capacities determined using the PSO model for Cu^{2+} removal agreed well to those determined experimentally. This suggests that in the adsorption of Cu^{2+} ions by CMC-stabilized nZVI particles, chemisorption [4] seems to be the rate-limiting step rather than diffusion. It could involve valence forces

through sharing or exchange of electron between the Cu²⁺ and CMC-stabilized nZVI particles. The Cu²⁺ ions adsorb on the CMC-stabilized nZVI particle surface forming chemical bonds and tend to find sites that maximize their coordination number with those particles. The rate constant of the PSO reaction is a complex function of the concentration of solute (Cu²⁺). The kinetic analysis reveals that the value of the initial adsorption rate, h is high at 10 mg/dm³ of Cu²⁺ concentration. In this case, high probability of collisions between the Cu species occurred and hence the probability increased for Cu²⁺ ions in the solution to be bonded to the active sites on the surface of the CMC-stabilized nZVI particles.

In medium acidic solutions, the corrosion of the CMC-stabilized nZVI particles accelerated, thereby enhancing the removal reaction. The initial pH values were 5.5, and 4.5, while after 240 min of reaction they increased to 6.4 and 4.68, respectively. This increase may be due to the oxidation of nZVI particles. The passivation on the nZVI surface at pH 4.5 and 5.5 confirmed the loss of reactivity and plateau on the removal curve. Therefore, the increase in pH will promote adsorption of Cr³⁺ ions and co-precipitation as mixed Fe³⁺-Cr³⁺ (oxy)hydroxides [3, 22]:



In addition, the mechanism of complex transformation of Cu²⁺ by CMC-stabilized nZVI particles involved physical adsorption followed by redox reaction, was considerably affected by pH of the solution. Redox potential occurred due to the higher oxidative ability of Cu²⁺ ($E^\theta = 0.33$ V) and the higher reductive ability of Fe⁰ ($E^\theta = -0.44$ V) [2]. At pH of 4.5, the removal of Cu²⁺ ions can occur directly on a fresh Fe⁰ surface after removal of iron oxides or hydroxides by H⁺ in the solution [22]. Cu and Cu₂O can form on the surface of nZVI particles after the removal process [3]. This finding conformed to the primary redox-type uptake mechanism, following equations:



In such a case, Cu²⁺ ions can be removed in the form of Cu⁰. However, small fractions may remain as Cu²⁺ ions.

The removal efficiencies of both heavy contaminants differ due to the different reduction potentials, E^θ (1.33 V for Cr⁶⁺ and 0.33 V for Cu²⁺) towards Fe⁰ as reductant at $E^\theta = -0.44$ V. In this case, Cr⁶⁺ acted as a more powerful oxidant compared to Cu²⁺.

However, due to adsorption of CMC-stabilized nZVI particles prior to the redox process, the obtained removal efficiency of Cu^{2+} was slightly higher at 94.65% (Fig. 6).

For the $\text{CMC}:\text{Fe}^{2+}$ molar ratio of 0.0034, the uptake of Cr^{6+} and Cu^{2+} by CMC-coated nZVI particles occurred on the Fe^0 surfaces, where Cr^{6+} and Cu^{2+} ions coordinated with the $-\text{COOH}$ and $-\text{OH}$ groups. The uptake process followed some mechanisms including (i) the complexation of ion pairing through electrostatic interactions or (ii) other specific interactions such as physical encapsulation in the interior cavities and interactions with trapped counter ions and/or water molecules [23]. Ionizable groups were likely formed by the electrostatic repulsion between the trapped Cr^{6+} and Cu^{2+} ions and free $-\text{COO}$ groups from the CMC monomers, in agreement with literature data [4]. This phenomenon further strengthened the binding of metal ions and increased Cr^{6+} and Cu^{2+} removal through adsorption and redox process. However, at higher $\text{CMC}:\text{Fe}^{2+}$ molar ratios, CMC monomers could cover significant number of reactive sites forming a compact coating on a surface, adversely affecting the accessibility target of Cr^{6+} or Cu^{2+} to reaction sites (Fe^0), which in turn results in decreased removal efficiency.

Without the ultrasonication procedure, the disadvantage of non-discrete particles (non-stabilized nZVI particles) caused by the magnetic forces [24], surface tension [25], electrical double-layer repulsion, and van der Waals attraction between iron species, as well as the attraction, hydration forces, and hydrophobic interaction between magnetic nanoparticles cannot be avoided [26]. These relatively resulted in lower Cr^{6+} and Cu^{2+} removal efficiencies. Low efficiency of the reaction of non-stabilized nZVI particles, was also caused by surface passivation which strongly limits electron transfer to reducible species (Fig. 6).

3.1.7. ADSORPTION BEHAVIOR OF Cr^{6+} AND Cu^{2+} ONTO THE CMC-STABILIZED nZVI PARTICLES

The adsorption isotherm shows the specific relationship between adsorbate concentration and the corresponding adsorption degree onto the adsorbent surface at a constant temperature. The linear dependences of C_e/A_m on C_e and $\log A_m$ on $\log C_e$ were plotted for the Langmuir and Freundlich isotherm models based on Eqs. (9) and (13) for adsorption process of Cr^{6+} and Cu^{2+} onto the 2.0 g/dm^3 CMC-stabilized nZVI particle surface at 30°C .

The Langmuir isotherm plot of C_e/A_m on C_e for the Cr^{6+} adsorption yielded the correlation coefficient $R^2 = 0.9769$, while that generated by the Freundlich isotherm $\log A_m$ vs. $\log C_e$ was only 0.8161 (Figs. 7a, b). These results confirmed that a monolayer was formed on the CMC-stabilized nZVI particle surface after reaching saturation. This model also predicted that the CMC-stabilized nZVI particle surface was energetically uniform with a finite number of identical sites with the maximum adsorption capacity, K_L of 0.7336 mg/g . The free energy (ΔG°) of the Cr^{6+} adsorption on CMC-stabilized nZVI particles calculated using Eq. (11) was -35.4992 kJ/mol . The negative value of ΔG° shows that the adsorption process was spontaneous.

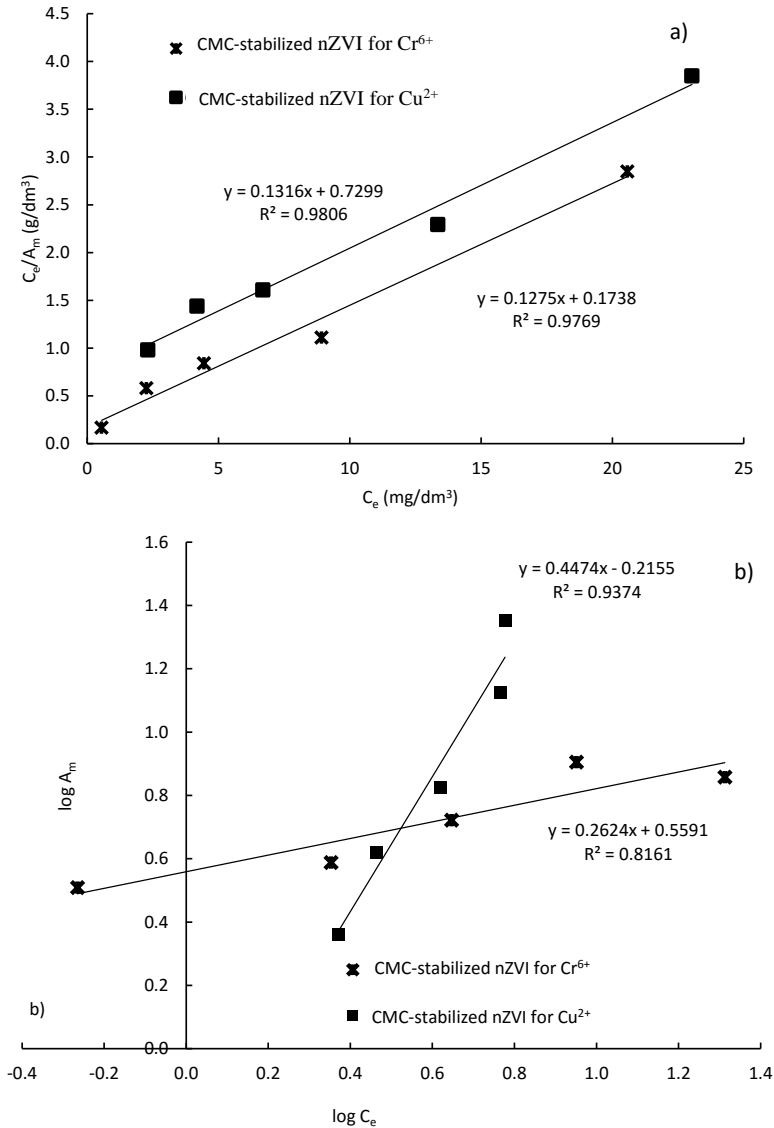


Fig. 7. The Langmuir (a) and the Freundlich (b) isotherms for the Cr^{6+} and Cu^{2+} at the concentration of 10 mg/dm^3

Therefore, the CMC-stabilized nZVI particles can be promising materials for Cr^{6+} removal in aqueous solutions. This result can be attributed to the higher surface area and average pore size of the nZVI particles. The larger surface area provided more adsorption sites to remove Cr^{6+} ions. The dimensionless equilibrium value, R_L was 0.0126 ($0 < R_L < 1$), fulfilling the conditions for a favorable adsorption process for Cr^{6+} removal.

The Langmuir isotherm for the Cu^{2+} adsorption generated a relatively higher regression coefficient (0.9768) compared with the Freundlich isotherm (0.9353) (Figs. 7a, b). Only a slight difference for the adjusted R^2 values was obtained, indicating that both isotherms fitted the data and were in close agreement with respect to the adsorption phenomenon. The homogenous moieties of the stabilizer in the nZVI particle suspension may be uniformly distributed across the surface. The observation herein also, strongly suggest that nZVI particles coordinated well with CMC at CMC: Fe^{2+} molar ratio of 0.0034, and formed a stable and well-dispersed aqueous solution after ultrasonication. The R_L values for the Langmuir isotherm were between 0.0249 and 0.0989, indicating that the Cu^{2+} removal by CMC-stabilized nZVI particles was favorable. In the Freundlich isotherm, the degree of nonlinearity constant (n) between Cu^{2+} concentration and adsorption was 3.0423, which represented favorable Cu^{2+} removal adsorption conditions. Apparently, the present result is inconsistent with that of Xiao et al. [4] who reported that the Langmuir model well described the Cu^{2+} removal using nZVI immobilized hybrid electrospun polymer nanofibrous mat.

3.1.8. SOLID PHASE CHARACTERIZATION OF Cr^{6+} AND Cu^{2+}
BY SCANNING ELECTRON MICROSCOPY (SEM) AND ENERGY-DISPERSIVE X-RAY SPECTROSCOPY (EDX)

SEM micrographs illustrate the pronounced corrosion effect and the formation of an oxide layer on the CMC-stabilized nZVI surface for both Cr^{6+} and Cu^{2+} ions (Fig. 8). Diffusion routes and reaction sites evolving on the oxide layers determined the removal rates. For comparison, SEM images of raw CMC-stabilized nZVI particles before the reduction process are shown in Figs. 8a, b. The surface layers of raw CMC-stabilized nZVI particles were coated with CMC stabilizers. The predominant morphology of those particles was initially euhedral and covered by outside layer of a stabilizer. The flake-like ions deposited and uniform rough surfaces (Figs. 8c, e) were visually visible after the initialization of the adsorption, redox and precipitation processes after Cr^{6+} removal. Obviously, after reaction the rough and exhausted surface layers formed due to the precipitation of metal hydroxides (Fe^{3+} - Cr^{3+}) on the spent surface of CMC-stabilized nZVI reflecting possible removal mechanism of Cr^{6+} [22]. This finding was also consistent with those obtained by Shi et al. [27]. Their reaction products were deposited on the surface of nZVI in the form of oxide-hydroxide co-precipitation of Fe(II), Fe(III) and Cr(III) through XRD analysis in the bentonite-supported nZVI system.

Similar to Cu^{2+} removal, evidence of corrosions on the spent iron surface was also found (Figs. 8d, f). Slightly porous, spongy, fragile, and flaky new particles formed on the surface of the nZVI particles collected after freeze-drying. The bright spots on the adsorbed particles may reflect prevalent copper deposition [28]. After phase separation, a typical black sample changed into a fragile brownish layer after ca. 10 days.

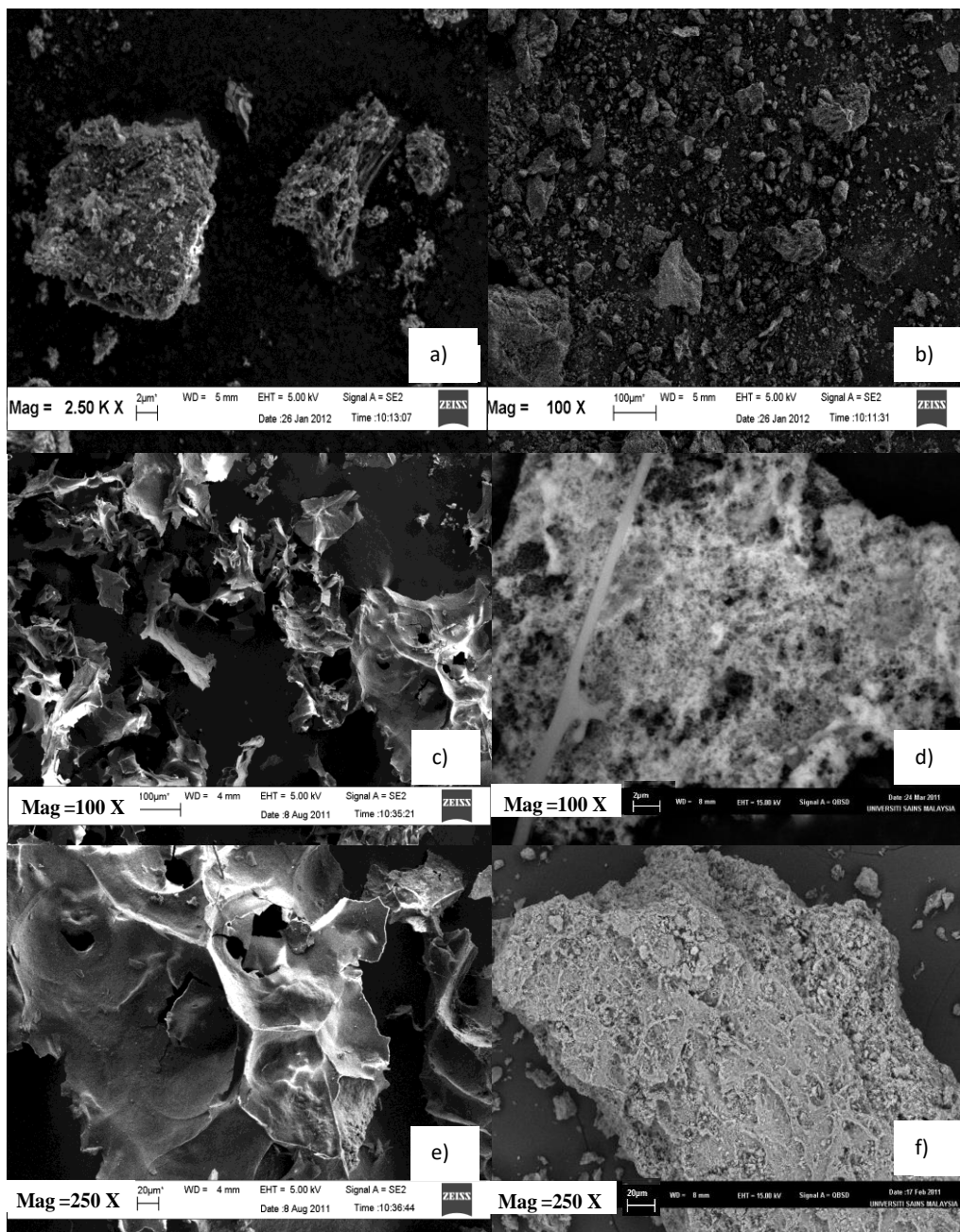


Fig. 8. SEM micrographs of: a), b) CMC-stabilized nZVI particles before reaction, c), e) surface corrosion after Cr^{6+} , d), f) Cu^{2+} absorbed onto the CMC-stabilized nZVI particles

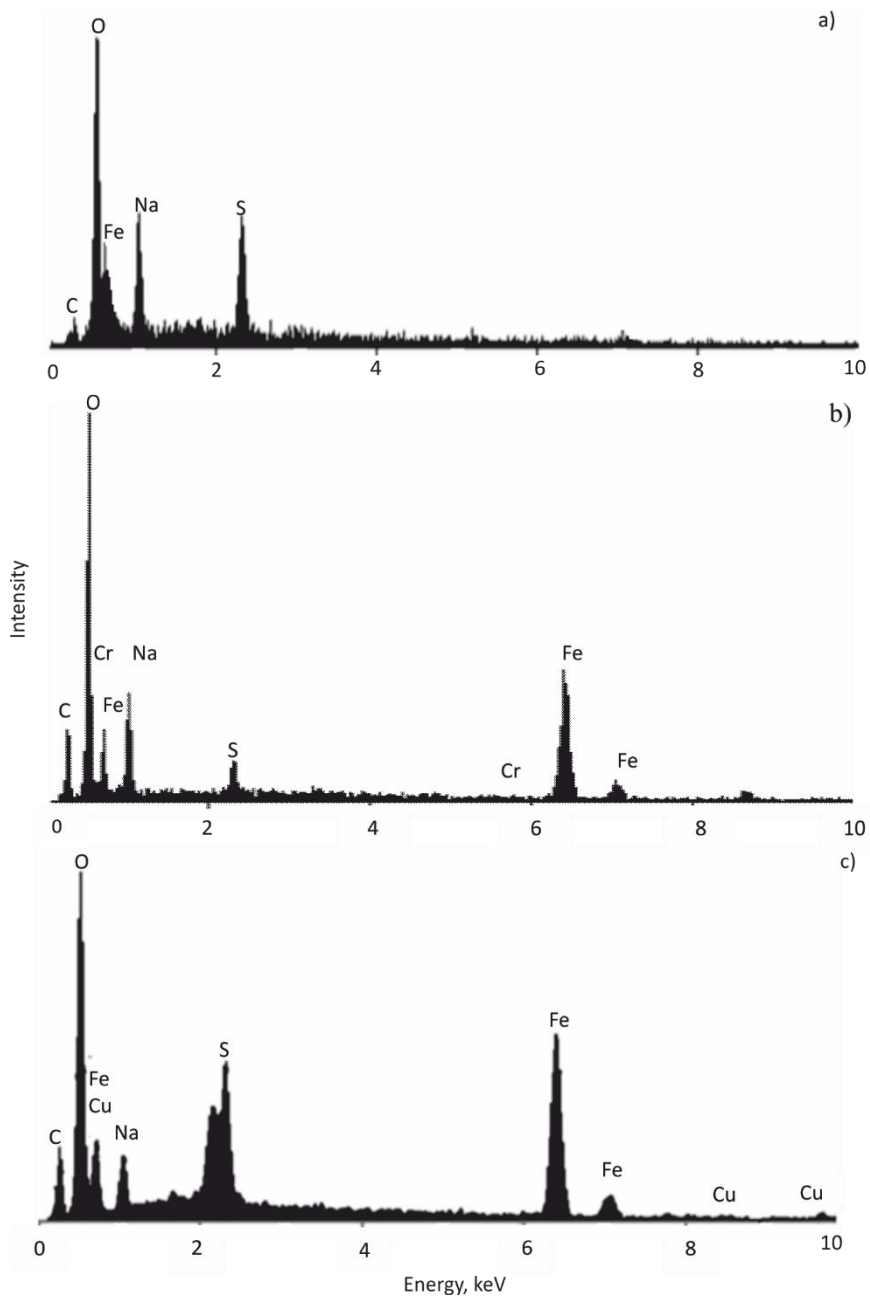


Fig. 9. EDX mapping of: a) CMC-stabilized nZVI particles before reaction, after Cr^{6+} (b) and Cu^{2+} (c) absorption onto 2.0 g/dm^3 CMC-stabilized nZVI particles

EDX spectra of randomly selected spots in fresh CMC-stabilized nZVI particle layer and on a spent nZVI surface were obtained to evaluate the presence of the corresponding element after reacting with Cr^{6+} and Cu^{2+} (Fig. 9a). The composition of the particles was inferred from the SEM images and amplitudes of various EDX peaks. From left to right, the specimen contained C, O, Na, and S, which are attributed to the CMC and precursor FeSO_4 compounds. The spectra show that fresh CMC-stabilized nZVI particles contained 11.01% of Fe, 27.99% of O, 25.52% of C, 0.13% of Na, and 15.53% of S (Fig. 9b). Therefore, the contents of O and C are significantly higher, according to CMC: Fe^{2+} molar ratio.

After the reaction with Cr^{6+} , Fe contents increased to 23.31%, and O, C, Na, and S were recorded at 38.44%, 27.68%, 2.75%, and 0.99% (Fig. 9b). The Cr signal appeared low (0.39%) between 5 and 6 keV, indicating that it was deposited onto exhausted semi-crystalline amorphous grains. Furthermore, the low Cr signal can also be caused by Cr^{6+} adsorption on the nZVI surface. For Cu^{2+} adsorption, the spectra indicate the sample contained 31.31% of Fe caused by corrosion. Other proportions of the components were 38.51% of O, 22.82% of C, 2.19% of Na, 4.37% of S and spectra with low (0.80%) Cu contents were recorded (Fig. 9c).

The higher contents of Fe – 43.44% and 31.31 for Cr^{6+} and Cu^{2+} , respectively, are expected, due to the oxidation and corrosion effect of nZVI in the aqueous medium. In addition, the higher Fe content could also result from the original molar ratio of CMC: Fe^{2+} at 0.005. Iron oxides or hydroxides and some co-precipitates of Fe–Cr and Fe–Cu on the surface of CMC-stabilized nZVI further increased the percentage of Fe. Simultaneously, the higher Fe composition obtained after Cr^{6+} reaction could be attributed to the higher reduction potentials ($E^\theta = 1.36$ V) as compared to Cu^{2+} ($E^\theta = 0.34$ V), at which direct electron transfers from nZVI particles were faster for more positive cations. The CMC-stabilized nZVI surface likely passivated more seriously under the effects of Cr^{6+} than that of Cu^{2+} (Figs. 8b, c), which could also be due to their different of reduction potentials.

4. CONCLUSIONS

This study has shown that CMC-stabilized nZVI can be used to remove Cr^{6+} and Cu^{2+} from aqueous solutions as the reactivity of CMC-stabilized is enhanced and the aggregation of nZVI reduced. The results of characterization indicated that CMC-stabilized onto the nZVI was well dispersed by using ultrasonication tool which regulated the redox chemistry in the solution and enhanced the removal rate constant. The removal reaction followed PFO and PSO models for Cr^{6+} and Cu^{2+} , respectively. Results of kinetic studies will be useful for future study of heavy metal treatment in contaminated subsurface water.

ACKNOWLEDGEMENTS

Funding from the Universiti Sains Malaysia Postgraduate Research Grant Scheme, grant No. 1001/PTEKIND/842002 is gratefully acknowledged.

REFERENCES

- [1] HOU M., WAN H., LUI T., LUI X., WAN X., *The effect of different divalent cations on the reduction of hexavalent chromium by zerovalent iron*, Appl. Catal. B Environ., 200, 84, 170.
- [2] KARABELLI D., UZUM C., SHAHWAN T., EROGLU A.E., SCOTT T.B., HALLAM K.R., LIEBERWIRTH I., *Batch removal of aqueous Cu^{2+} using nanoparticles of zero-valent iron. A study of the capacity and mechanism of uptake*, Ind. Eng. Chem. Res., 2008, 47, 4758.
- [3] GHEJU M., BALCU I., *Removal of chromium from Cr(VI) polluted wastewaters by reduction with scrap iron and subsequent precipitation of resulted cations*, J. Hazard. Mater., 2011, 196, 131.
- [4] XIAO S., MA H., SHEN M., WANG S., HUANG Q., SHI X., *Excellent copper(II) removal using zero-valent iron nanoparticle-immobilized hybrid electrospun polymer nanofibrous mats*, Colloid Surface A, 2011, 381, 48.
- [5] CRANE R.A., SCOTT T.B., *Nanoscale zero-valent iron. Future prospects for an emerging water treatment technology*, J. Hazard. Mater., 2012 (211/212), 112.
- [6] DICKSON D., LIU G., LI C., TACHIEV G., CAI Y., *Dispersion and stability of bare hematite nanoparticles: Effect of dispersion tools, nanoparticles concentration, humic acid and ionic strength*, Sci. Total Environ., 2012, 419, 170.
- [7] CRANE R.A., DICKINSON M., POPESC I.C., SCOTT T.B., *Magnetite and zero-valent iron nanoparticles for the remediation of uranium contaminated environmental water*, Water Res., 2011, 45 (9), 2931.
- [8] O'CARROLL D., SLEEP B., KROL M., BOPARAI H., KOCUR C., *Nanoscale zero valent iron and bimetallic particles for contaminated site remediation*, Adv. Water Res., 2013, 51, 104.
- [9] HE F., ZHAO D., *Manipulating the size and dispersibility of zerovalent iron nanoparticles by use of carboxymethyl cellulose stabilizers*, Environ. Sci. Technol., 2007, 41, 6216.
- [10] HE F., ZHAO D., *Preparation and characterization of a new class of starch-stabilized bimetallic nanoparticles for degradation of chlorinated hydrocarbons in water*, Environ. Sci. Technol., 2005, 39, 3314.
- [11] JANARDHANAN S.K., RAMASAMY I., NAIR B.U., *Synthesis of iron oxide nanoparticles using chitosan and starch templates*, Transit. Metal Chem., 2008, 33, 127.
- [12] CHEREPY N.J., LISTON D.B., LOVEJOY J.A., DENG H., ZHANG J.Z., *Ultrafast studies of photoexcited electron dynamics in γ - and α - Fe_2O_3 semiconductor nanoparticles*, J. Phys. Chem. B, 1998, 102, 770.
- [13] SYLVESTER J.P., POULIN S., KABASHIN A.V., SACHER E., MEUNIER M., LUONG J.H.T., *Surface chemistry of gold nanoparticles produced by laser ablation in aqueous media*, J. Phys. Chem. B, 2004, 108 (43), 16864.
- [14] HUANG K.C., EHRMAN S.H., *Synthesis of iron nanoparticles via chemical reduction with palladium ion seeds*, Langmuir, 2007, 23 (3), 1419.
- [15] BAER D.R., GASPAR D.J., HACHIMUTHU P., TECHANE S.D., CASTNER D.G., *Application of surface chemical analysis tools for characterization of nanoparticles*, Anal. Bioanal. Chem., 2010, 396 (3), 983.
- [16] BRULLOT W., REDDY N.K., WOUTERS J., VALEV V.K., GODERIS B., VERMANT J., VERBIEST T., *Versatile ferrofluids based on polyethylene glycol coated iron oxide nanoparticles*, J. Magn. Mater., 2012, 324, 1919.
- [17] GREENLEE L., HOOKER S.A., *Development of stabilized zero valent iron nanoparticles*, Desalination Water Treat., 2012, 37, 114.

- [18] PHENRAT T., SALEH N., SIRK K., KIM H.J., TILTON R.D., LOWRY G.V., *Stabilization of aqueous nanoscale zerovalent iron dispersions by anionic polyelectrolytes. adsorbed anionic polyelectrolyte layer properties and their effect on aggregation and sedimentation*, J. Nanopart. Res., 2008, 10 (5), 795.
- [19] LIN C.L., LEE C.F., CHIU W.Y., *Preparation and properties of poly (acrylic acid) oligomer stabilized superparamagnetic ferrofluid*, J. Interf. Sci., 2005, 29, 411.
- [20] DICKINSON M., SCOTT T.B., *The application of zero-valent iron nanoparticles for the remediation of a uranium-contaminated waste effluent*, J. Hazard. Mater., 2010, 178, 171.
- [21] LI L., QUINLIVAN P.A., KNAPPE D.R.U., *Effects of activated carbon surface chemistry and pore structure on the adsorption of organic contaminants from aqueous solution*, Carbon, 2002, 40, 2085.
- [22] PETALA E., DIMOS K., DOUVALIS A., BAKAS T., TUCEK J., ZBOŘIL R., KARAKASSIDES M.A., *Nanoscale zero-valent iron supported on mesoporous silica. Characterization and reactivity for Cr(VI) removal from aqueous solution*, J. Hazard. Mater., 2013, 261, 295.
- [23] ZHAO X., LV L., PAN B., ZHANG W., ZHANG S., ZHANG Q., *Polymer-supported nanocomposites for environmental application. A review*, Chem. Eng. J., 2011, 170, 381.
- [24] KORTH B.D., KENG P., SHIM I., BOWLES S.E., TANG C., KOWALEWSKI T., NEBESNY K.W., PYUN J., *Polymer-coated ferromagnetic surfactants and assembly into nanoparticle chains*, J. Am. Chem. Soc., 2006, 128, 6562.
- [25] WANG Q., LEE S., CHOI H., *Aging study on the structure of Fe-O nanoparticles. Stabilization, characterization, and reactivity*, J. Phys. Chem. C, 2010, 114 (5), 2027.
- [26] ELIMELECH M., GREGORY J., JIA X., WILLIAMS R., *Particles deposition and aggregation. Measurement, modeling, and simulation*, Butterworth-Heinemann, Boston, 1995.
- [27] SHI L.-N., ZHANG X., CHEN Z.-L., *Removal of chromium(VI) from wastewater using bentonite-supported nanoscale zero-valent iron*, Water Res., 2011, 45, 886.
- [28] RANGSIVIEK R., JEKEL M.R., *Removal of dissolved metals by zero-valent iron (ZVI). Kinetics, equilibria, process and implications for stormwater runoff treatment*, Water Res., 2005, 39, 4153.